

PAPER • OPEN ACCESS

Selective area intermixing of III–V quantum-dot lasers grown on silicon with two wavelength lasing emissions

To cite this article: Mengya Liao *et al* 2019 *Semicond. Sci. Technol.* **34** 085004

View the [article online](#) for updates and enhancements.



IOP | ebooks™

Bringing you innovative digital publishing with leading voices to create your essential collection of books in STEM research.

Start exploring the collection - download the first chapter of every title for free.

Selective area intermixing of III–V quantum-dot lasers grown on silicon with two wavelength lasing emissions

Mengya Liao^{1,3,4} , Wei Li^{2,3}, Mingchu Tang¹, Ang Li², Siming Chen^{1,4}, Alwyn Seeds¹ and Huiyun Liu¹ 

¹ Department of Electronics and Electrical Engineering, University College London, London WC1E 7JE, United Kingdom

² Institute of Microstructure and Properties of Advanced Materials, Beijing University of Technology, Beijing 100124, People's Republic of China

E-mail: mengya.liao@ucl.ac.uk and siming.chen@ucl.ac.uk

Received 17 April 2019, revised 20 May 2019

Accepted for publication 24 June 2019

Published 5 July 2019



CrossMark

Abstract

The ability to tailor the bandgap of III–V compound semiconductors spatially, across the wafer is highly desirable for monolithically integrating photonic components with multi-functions. Using rapid thermal annealing with SiO₂ and TiO₂ capping layers as a selective area intermixing technique, we have demonstrated selective area bandgap tuning of III–V quantum dot (QD) material on a silicon (Si) substrate. Electrically pumped InAs/GaAs QD lasers directly grown on Si with dual-wavelength lasing emissions of 1275 and 1313 nm have been fabricated by this technique. This result indicates that the selective area intermixing technique can potentially be used in optical integrated circuits for Si photonics.

Keywords: quantum-dot laser, intermixing, silicon photonics

(Some figures may appear in colour only in the online journal)

1. Introduction

Silicon (Si) photonics-enabled optical interconnections is one of the strongest candidates to replace traditional copper interconnections in information systems. It allows information transfer via photons rather than electrons, thus with a much faster transmission speed, higher throughput and lower power dissipation [1–3]. Among the various kinds of well-studied Si optical components, Si-based light source emitters, which had been considered as a road-block for Si photonics [4], have now been achieved a by integrating III–V lasers on

Si platforms, using wafer bonding methods [4–7] and epitaxial growth methods [8–12]. Although the former approach has already shown the nearly commercialised laser results, the latter one can provide ultimate integration density and the advantages of high volume manufacture [13]. The biggest hurdle for monolithic integration is the dissimilarities between III–V compounds and Si materials, which introduce a high density of defects, leading to reduced device performance and device lifetime limitations. By applying the combined strategies of mitigation of various defects and using III–V quantum dots (QDs) as the active region, practical and reliable InAs/GaAs QD lasers directly grown on off-cut Si/‘on-axis’ (001) Si with long lifetimes have been reported recently [10, 12]. The driving forces for the utilisation of QDs are not only their high efficient light generation rate (ultra-low threshold current) and temperature-insensitive properties, but also the enhanced tolerance to defects, due to the strong carrier localisation within the QDs [14]. Thus, it is clear that the QD is an ideal active structure for III–V lasers directly

³ These authors contributed equally to this work.

⁴ Authors to whom any correspondence should be address.



Original content from this work may be used under the terms of the [Creative Commons Attribution 3.0 licence](https://creativecommons.org/licenses/by/3.0/). Any further distribution of this work must maintain attribution to the author(s) and the title of the work, journal citation and DOI.

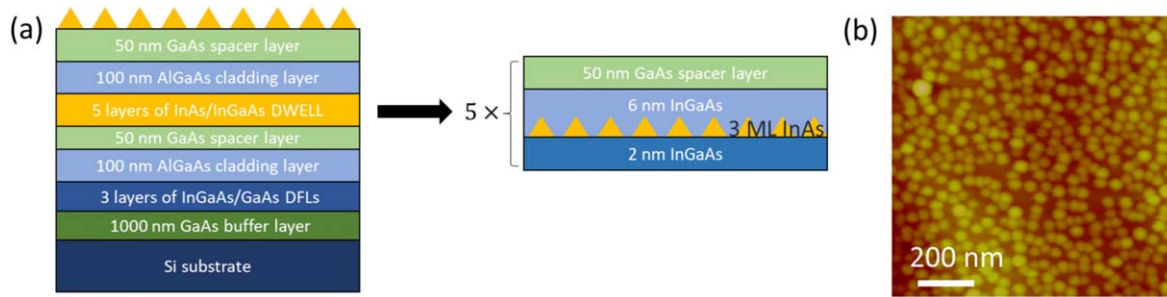


Figure 1. (a) Schematic of InAs/GaAs DWELL epitaxy layers directly grown on Si substrate with thin cladding layers. (b) AFM image of un-capped InAs/GaAs QD directly grown on Si with $3 \times 10^8 \text{ cm}^{-2}$ of dot density.

grown on Si [15]. Recently, the dynamic properties of III–V/Si QD lasers have also been studied, in terms of relative intensity noise [16, 17], modulation bandwidth [18, 19], gain switching [20] etc. These results demonstrate the high potential of Si-based III–V QD lasers to be used as on-chip light sources for Si photonics.

To realise a monolithically integrated photonic circuit, the ability to engineer the bandgap across the wafer spatially is one of the critical points to reduce optical loss in waveguides [21]. In general, multiple bandgaps can be approached by two methods: selective area epitaxial regrowth or intermixing techniques [22]. The intermixing approach by rapid thermal annealing (RTA) is a relatively simple approach, compared with regrowth and widely used in modifying the wavelength of materials, either for quantum-wells [22–24] or QDs [25–29]. Among the various intermixing methods, impurity-free vacancy disordering assisted by dielectric layers is particularly attractive for optical integrated circuit fabrication, because it does not involve the introduction of extra impurities or damage [21]. The dielectric layers, which were deposited on the top of III–V epitaxy layers, play an important role in controlling the intermixing levels by their different thermal expansion coefficients. A thin layer of SiO_2 with thermal expansion coefficient of $0.52 \times 10^{-6} \text{ }^\circ\text{C}^{-1}$ has been shown to produce a significant enhancement of the intermixing when it was capped on InAs/GaAs QD structure [27]. Due to the thermal expansion coefficient mismatch between GaAs ($\sim 6.5 \times 10^{-6} \text{ }^\circ\text{C}^{-1}$) and SiO_2 , a compressive strain is produced at the interface of GaAs/ SiO_2 induces Ga atoms to migrate into the SiO_2 cap. Ga vacancies created by the enhanced Ga migration are then diffused through the III–V epi-structures and cause the intermixing process (blue shift) at the active region. In comparison with SiO_2 , the TiO_2 layer has a much larger thermal expansion coefficient of $\sim 8.2 \times 10^{-6} \text{ }^\circ\text{C}^{-1}$ than GaAs, a tensile strain at the interface will restrict Ga vacancies produced during RTA, thus suppressing the inter-diffusion rate [30]. Therefore, the multiple bandgaps of III–V QD materials could be achieved by lateral patterning SiO_2 and TiO_2 on top before the RTA process, to provide a selective area intermixing technique. Using this technique, we can intentionally engineer the bandgap for individual photonic devices, such as QD lasers, electro-absorption modulators and low-loss waveguides, all monolithically integrated on the same platform. Although there are significant pioneering works on the selective area intermixing

studies for QD materials on native substrates [27, 30], the intermixing effect of III–V QDs monolithically grown on a Si substrate, which may become more complicated due to the high-density defects involved, have not been reported in detail previously.

In this paper, a comparative study of the intermixing effect in InAs/GaAs QDs directly grown on Si capped by separated SiO_2 and TiO_2 layers, to determine the optimal thermal annealing conditions, is reported first. Detailed analysis of annealed QDs with different temperatures of the two capping layers, in terms of physical shape, sizes and size distributions, have been evaluated by using high-resolution aberration (C_s) corrected scanning transmission electron microscopy (STEM). Based on the optimised annealing conditions from each individual study, the III–V/Si QD structure material with double bandgaps has been achieved by using the selective area intermixing technique. Thus, electrically pumped InAs/GaAs QD lasers directly grown on Si with two different emission wavelengths of 1275 and 1313 nm have been fabricated from this thermally processed wafer, showing that this selective area intermixing technology can be used in optical integrated circuits for Si photonics without severe degeneration of the QD material quality.

2. Experiment methods

2.1. Optimisation of RTA conditions for SiO_2 and TiO_2 capped samples

In this work, as shown in figure 1(a), the III–V QD structure was grown by a molecular beam epitaxy system on the n-doped Si (001) substrate with an oriented offset of 4° towards the [110] direction. A 6 nm AlAs nucleation layer was deposited first to provide a good interface between Si and III–V materials [31]. After a 1000 nm GaAs buffer layer and three layers of five periods of InGaAs/GaAs strained-layer superlattices as dislocation filter layers, the threading dislocation (TD) density was reduced from the order of 10^9 cm^{-2} to the order of 10^7 cm^{-2} ; detailed descriptions can be found in [9, 32]. To gain a better understanding of the emission properties of the QDs from photoluminescence (PL) measurement, very thin AlGaAs upper and lower cladding layers of 100 nm are used for this test sample. In the active region,

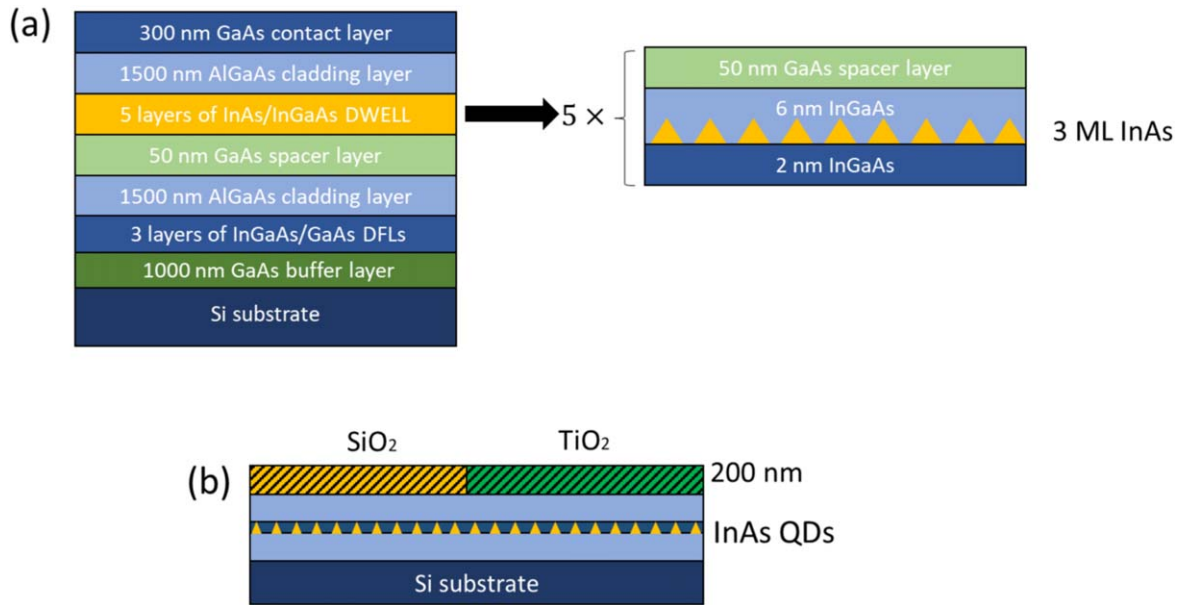


Figure 2. (a) Schematic of InAs/GaAs DWELL laser structure directly grown on Si substrate. (b) Schematic of cross-section of SiO₂ and TiO₂ dielectric layer on III-V/Si QDs for selective area intermixing.

five layers of dot-in-a-well (DWELL) structure was grown, separated by 50 nm GaAs spacer layers. Each layer of DWELL consists of 2 nm InGaAs wetting layer, 3ML InAs QDs and 6 nm InGaAs capping layer. On top of the sample, uncapped 3ML InAs QDs were grown for QD density measurement using an atomic force microscope (AFM). Figure 1(b) shows the AFM image of QD density, which is around $3 \times 10^8 \text{ cm}^{-2}$.

Before the thermal annealing process, the sample was cleaved into two and capped with a 200 nm SiO₂ film by plasma-enhanced chemical vapour deposition and 200 nm TiO₂ film by physical vapour deposition (PVD75), respectively. The two samples were then cleaved into many pieces for further comparison studies. For the SiO₂-capped samples, an RTA duration study was implemented for 0, 5, 30, 60 s at 700 °C. Based on the optimal annealing duration, different annealing temperatures of 700 °C, 725 °C, 750 °C, 775 °C and 800 °C were trialled. The annealing temperature study for TiO₂-capped samples was then executed at 700 °C, 725 °C, 750 °C and 775 °C. PL measurements of each as-grown and annealed sample were conducted under excitation using a solid-state laser of wavelength 532 nm at room temperature (RT).

For better understanding the effect of intermixing on the QDs capped by SiO₂ and TiO₂, high angle annular dark field (HAADF) STEM images were obtained using a C-FEG JEOL R005 double aberration corrected TEM/STEM operating at 300 kV. Lattice resolved STEM HAADF Z-contrast images, were then obtained with a convergence semi-angle of 21 mrad and a STEM inner annular collection angle of 62 mrad.

2.2. Selective area intermixing and laser device fabrication

For the selective area intermixing, the real laser structure of InAs/GaAs QDs on Si substrate was grown as shown in figure 2(a). The epitaxy layers and growth method were identical to the previous test sample, except for the two thick cladding layers of 1.5 μm and a highly doped 300 nm GaAs contact layer on the top. A quarter of the wafer was then covered by 200 nm SiO₂ and TiO₂ thin film half and half as shown in figure 2(b). A trade-off RTA condition of duration and temperature was applied from the previous optimisation studies for both SiO₂ and TiO₂ caps. After thermal annealing, PL mapping was executed to check the bandgap changes of the QD materials. The dielectric layers were then removed using hydrofluoric acid (HF) before further device fabrication. 25 μm width broad area lasers were fabricated by standard photolithography, wet chemical etching and metallisation. Ti/Pt/Au and Ni/GeAu/Ni/Au were deposited for p-type and n-type ohmic contacts, respectively. The laser devices were then cleaved into 3 mm length cavities, without any facet coatings, and mounted on the copper heatsinks.

3. Results and discussion

3.1. SiO₂ capping

3.1.1. PL spectra. Figure 3(a) shows RT PL spectra of the intermixing duration study of DWELL structure capped by SiO₂ for as-grown (A.G.), 5, 30 and 60 s RTA. The inset of figure 3(a) shows the PL peak intensity as a function of the annealing duration, showing an increase with longer annealing time and reaching the maximum point when the duration is 30 s. The increased PL intensity is contributed to by the reduced TD density after the high RTA. The high-temperature annealing enhances the mobility of dislocations

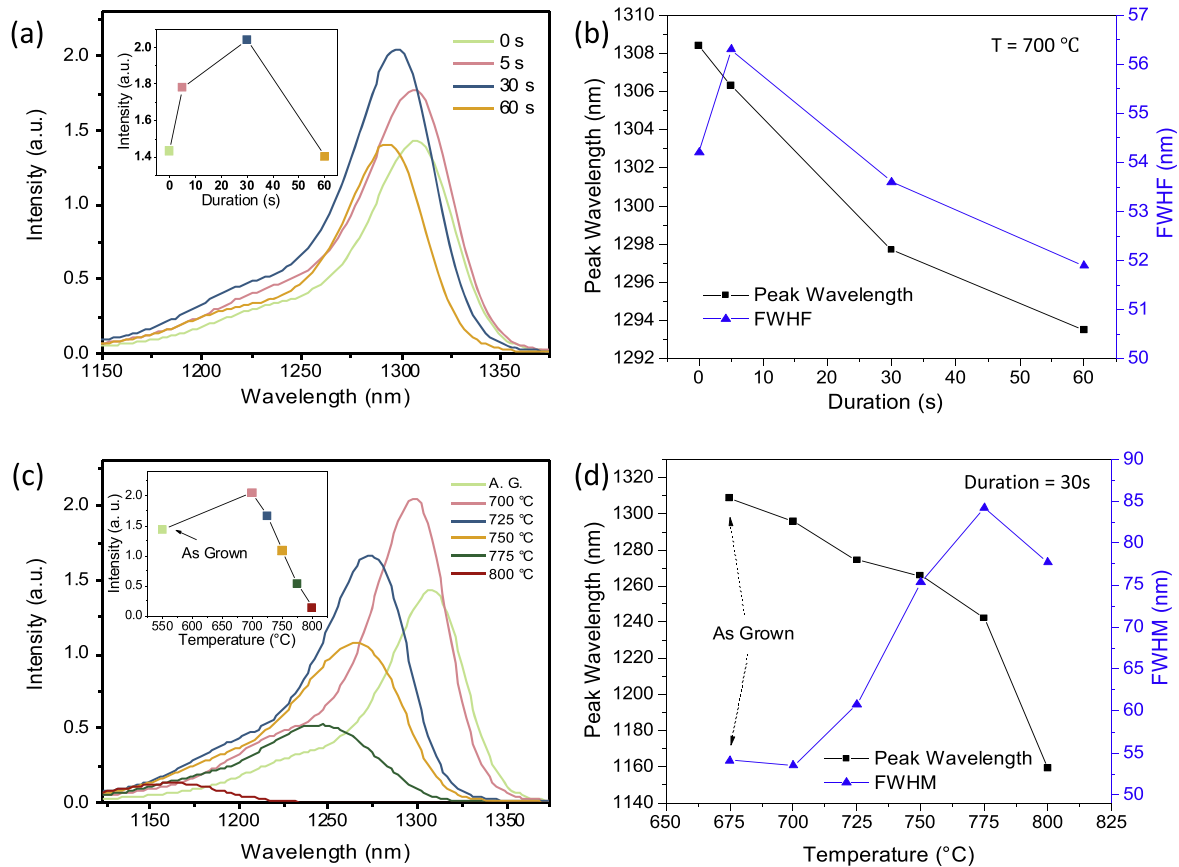


Figure 3. (a) PL spectra of SiO₂ capped InAs/GaAs DWELL structure grown on Si substrate with different duration times at 700 °C. Inset: the PL intensity against to the annealing durations. (b) Plots of PL peak wavelength and FWHM against to the annealing durations at 700 °C. (c) PL spectra of SiO₂ capped InAs/GaAs DWELL structure grown on Si substrate with 30 s duration at different temperatures. Inset: the PL intensity against to the annealing temperature. (d) Plots of PL peak wavelength and FWHM against to the annealing temperatures with 30 s duration.

and increases the probability of interaction and self-annihilation of the TDs with each other [33]. As shown in figure 3(b), the peak wavelength of PL was decreased with increased annealing time. This small blue shift is due to the inter-diffusion of In and Ga atoms between the interface of InAs QDs and GaAs barrier layers. The change of full width at half maximum (FWHM) of PL for the duration study is also shown in figure 3(b), the FWHM is raised at first when the annealing time is 10 s, and then decreases with longer annealing times. The decreased FWHM indicates an improved QDs size homogeneity when the annealing time is longer than 30 s. By considering the peak intensity, wavelength and FWHM, an annealing time of 30 s was chosen for the subsequent annealing temperature study, as it shows a relatively larger blue-shift and peak PL intensity.

Figure 3(c) shows the PL spectra of the annealing temperature study from 700 °C to 800 °C with 25 °C intervals for 30 s annealing duration. At first, the intensity of PL is increased and reaches the maximum point when the annealing temperature is 700 °C, it then decreases gradually as the annealing temperature is increased further (inset of figure 3(c)). Although the RTA can help to reduce the TD density, higher annealing temperature can degenerate the material quality, thus causing a dramatic PL intensity decline

[34]. The high temperature also causes a bigger blue shift of PL emission, and a comparison of peak wavelengths at different temperatures is shown in figure 3(d). It should be noticed that the PL spectra become broader when the annealing temperature is raised from 725 °C to 775 °C. However, the linewidth narrows at a very high temperature of 800 °C from figure 3(d). The broader linewidth accompanied by the large blue-shift is the contribution from an inhomogeneous diffusion of Ga atoms at relatively low annealing temperature [35]. Therefore, we presume that the RTA leads to a distinct change of emission peak and an increased linewidth at relatively low temperatures with SiO₂ cap. At 800 °C, the influence of annealing on size distribution is more dominant. As a result, the FWHM reduces again, and the blue shift of the PL spectrum becomes larger than at other temperatures. This conclusion is further confirmed by our STEM observations.

The purpose of these studies is to find the most suitable RTA conditions, in terms of annealing time and temperature, of the SiO₂-capped DWELL structure for a relatively large wavelength shift and an appropriate QDs optical emission without serious material degradation. By considering results from both annealing time and temperature studies, the RTA with 30 s duration at 725 °C causing ~34 nm blue-shift in PL

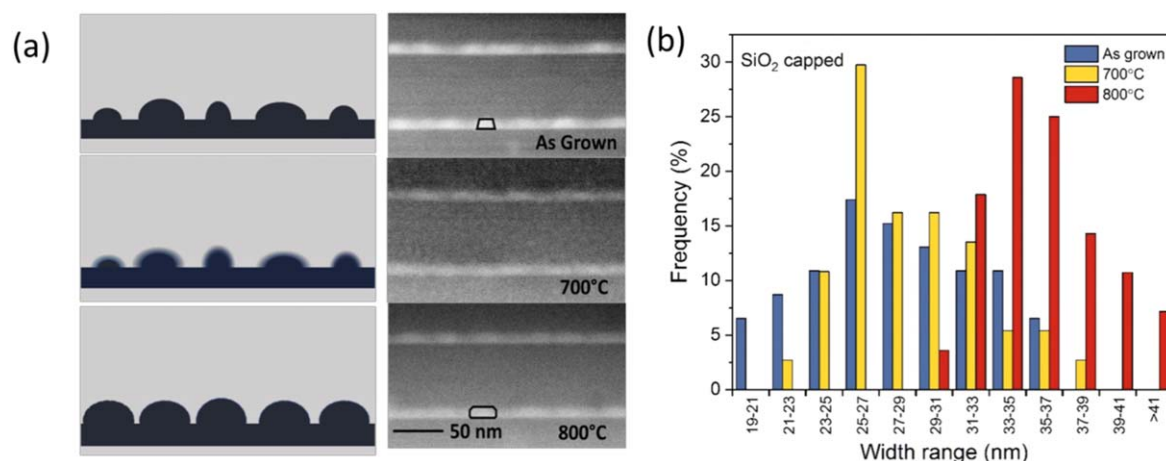


Figure 4. (a) C_s corrected HAADF STEM images of SiO₂ capped DWELL as a function of annealed temperature and related schematic diagram. (b) Histogram of SiO₂ capped QDs widths in as-grown, 700 °C annealed and 800 °C annealed samples.

Table 1. Summary the widths, heights and height/width ratio of SiO₂ capped QDs in as grown, 700 °C and 800 °C annealed samples.

Sample	Width (nm)	Height (nm)	Height/width ratio
As grown	28.2 ± 4.4	8.8 ± 1.0	0.31
700 °C	28.8 ± 3.7	9.0 ± 0.8	0.31
800 °C	36.0 ± 3.3	9.5 ± 0.9	0.26

peak position and ~15.9% increases in PL intensity is the most useful choice, which is the reference for the further RTA study for the TiO₂-capped DWELL and selective area intermixing.

3.1.2. QD morphologic and size distribution analysis.

HAADF STEM images of as-grown and annealed specimens were obtained at relatively low magnification (at ~600kX, for size distribution analysis) while detailed STEM images of individual QD's have been taken at high magnification (at ~4MX) for comparison. As the image contrast in the HAADF image is approximately proportional to the square of the mean atomic number, assuming pure Rutherford scattering, such images offer an insight into the relative local chemistry of the features.

Figure 4(a) shows the HAADF STEM images for SiO₂ capped DWELL of the as-grown, 700 °C and 800 °C annealed samples and a corresponding schematic diagram of the morphological evolution. As the images are shown, QDs in the as-grown sample exhibit a sharp interface and inhomogeneous dot size. After 700 °C annealing, the interface of QDs and the surrounding matrix became less distinct, possibly due to the thermally intermixing process. However, after 800 °C annealing, the QD uniformity had significantly improved, with an increase in the average dot-size.

Approximately 100 QDs have been measured for each of the as-grown, 700 °C annealed and 800 °C annealed samples using HAADF imaging at ~600 k magnification to determine the width and height of the QDs. The widths and heights of the QDs were measured by drawing intensity line profiles across the HAADF images. Table 1 displays the widths,

heights and height/width ratio of QDs in the as-grown, 700 °C and 800 °C annealed samples. The widths of QDs in 700 °C and 800 °C annealed samples increase by 2.1% and 27.7% respectively. On the other hand, the heights do not appear to change significantly, when measurement error is taken into consideration. This phenomenon would suggest the inter-diffusion predominates within the (100) plane rather than the [100] growth direction. Considering the theoretical QD geometries proposed in [36, 37], this means the ratio between the height h and the base length b is smaller after the post-growth annealing.

A more detailed width distribution of QDs capped by SiO₂ is given by the histogram presented in figure 4(b). The standard deviation of the 100 QDs size from the as-grown sample is around 4.4 nm. After the high-temperature thermal annealing, the standard deviation is decreased to 3.7 nm, and 3.3 nm from 700 °C and 800 °C annealed samples, respectively. These results are evidence to support our previous assumption from the PL measurement. The improved uniformity of QD size distribution after the RTA is the contribution of the decrease of FWHM at 700 °C and 800 °C.

Figure 5 shows a series of lattice resolved HAADF STEM Z-contrast images (presented in false colour) of typical single QDs as a function of annealing temperature. The increased contrast brightness in the region of the QD reflects the higher mean atomic number due to the presence of Indium. While the Z-contrast images are not specifically indium concentration maps, they highlight the changes in the QD morphology, which is likely to be associated with localised indium diffusion. The typical as-grown dot is ~25 nm in diameter. After 700 °C annealing, the image contrast becomes more uniform across the dot region, and the QD size increased lateral. After 800 °C annealing, the lateral dot size further increased. It is important to note that although the overall aspect ratio appears to change as a function of annealing temperature, the basic shape morphology of QDs remains essentially the same.

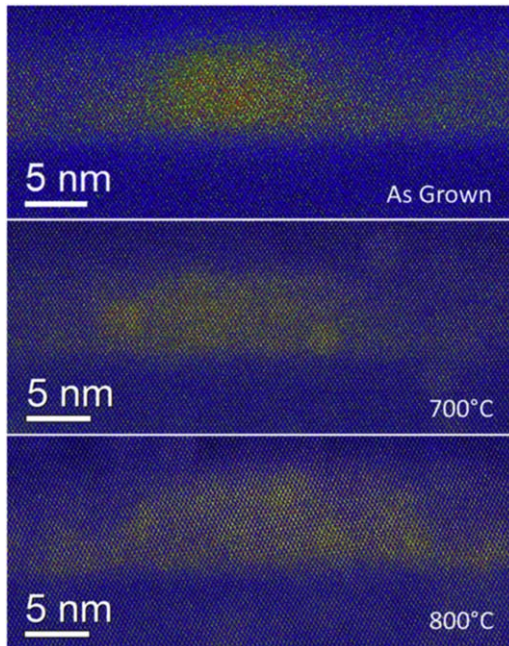


Figure 5. C_s corrected high resolution HAADF STEM images (shown in false colour) of a single QD of SiO_2 capped DWELL as a function of annealed temperature with 30 s duration.

3.2. TiO_2 capping

3.2.1. PL spectra. Due to the larger thermal expansion coefficient of TiO_2 , the inter-diffusion rate inside of the TiO_2 capped DWELL structure is restricted during the RTA. Figure 6(a) shows the comparison of the PL spectra between the as-grown and TiO_2 -capped DWELL structures with 30 s anneal duration at different temperatures from 700 °C to 775 °C. Since the annealing temperature of 800 °C is too high to maintain the material quality for SiO_2 cap, 800 °C is not employed in the following studies. The inset of figure 6(a) is the plot of the peak intensity of PL as a function of annealing temperature. The peak intensity is first raised and reached its maximum point at 700 °C, then reducing as the temperature increased. The intensity trace of the TiO_2 cap is similar to the SiO_2 annealing temperature study, where an appropriate annealing temperature could enhance the self-annihilation of the dislocations, thus improving the PL intensity. As the temperature further increased, the material quality and QDs will be degenerated or destroyed, gradually causing the PL intensity to drop. Comparing with the SiO_2 -capped DWELL, the TiO_2 -capped DWELL shows a much smaller blue-shift under the same annealing conditions, as demonstrated in figure 6(b). The blue-shift of TiO_2 -capped DWELL structure is only ~6.4 nm by RTA for 30 s at 725 °C. Also, the FWHM has a slight decrease at temperature up to 725 °C owing to the narrower size distribution of QDs.

3.2.2. QD morphologic and size distribution analysis.

Figure 7(a) shows the HAADF STEM images of the DWELL of the as-grown, 700 °C annealing 775 °C annealing samples capped by TiO_2 , with a corresponding schematic diagram of morphological evolution shown at the

left-hand side. Comparing with the SiO_2 capped DWELL, the QDs capped by TiO_2 still retained the sharp interface and inhomogeneous dot size even after 700 °C annealing. When the annealing temperature increased to 775 °C, the surrounding matrix of dots became less distinct, and the average dot size was slightly increased due to the intermixing process at a very high temperature. This intermixing phenomenon has happened at 700 °C for SiO_2 capped QDs, which evidences that the TiO_2 with a larger thermal expansion coefficient could effectively restrict the intermixing process.

Table 2 shows the average size of QDs in width and height for as grown, 700 °C and 775 °C annealed samples. The widths of TiO_2 capped QDs for 700 °C, and 775 °C annealed samples are increased by 1.9% and 11.5%, respectively, compared with the as-grown sample. The error bars were calculated from the standard deviation, where the insignificant changes for different annealing temperature samples mean the size distribution of TiO_2 capped QDs for each sample remained almost the same. A detailed histogram of TiO_2 capped QDs widths in as-grown, 700 °C annealed and 775 °C annealed samples is shown in figure 7(b).

The HAADF STEM Z-contrast images of typical QDs as a function of annealing temperature are shown in figure 8. The indium distribution of a single dot is highlighted with contrast brightness. For TiO_2 -capped QDs, the image contrasts of the single QDs of the as-grown sample and the 700 °C annealed sample are almost unchanged. Only a slight indium diffusion happens at the edge of QD at 700 °C annealing due to the intermixing process. After 775 °C annealing, the indium diffusion became more pronounced. Although it still keeps a basic shape morphology, the dot lateral dimension increases further as with the SiO_2 capped QD annealed at temperatures above 700 °C. The TEM results are consistent with the observation from the PL measurements in figure 6.

3.3. Selective area intermixing and laser results

Based on the previous studies of the annealing conditions of SiO_2 and TiO_2 caps, the RTA process with 30 s duration at 725 °C was implanted for selective area intermixing. Figure 9(a) shows the PL mapping of the peak wavelength for a QD wafer sample after the RTA with the SiO_2 and TiO_2 capped regions labelled. A clear square pattern could be found on the right side of the sample, which was covered by TiO_2 . As expected from the previous studies, the SiO_2 capped region shows a bigger wavelength shift in PL measurement comparing with the TiO_2 capped region. Also, an even larger wavelength shift and a reduced intensity were obtained on the edge of the SiO_2 capped region. It is likely that the RTA caused serious degradation of the material quality at the wafer edge. Figures 9(b) and (c) show the comparisons of the PL spectra at the centres of SiO_2 and TiO_2 capped regions before and after RTA, respectively. Table 3 summarises the wavelength-dependent results of the PL spectra. There is a ~40 nm blue shift of wavelength at the SiO_2 capped region after RTA, and only ~3.4 nm peak wavelength shift at the TiO_2 capped

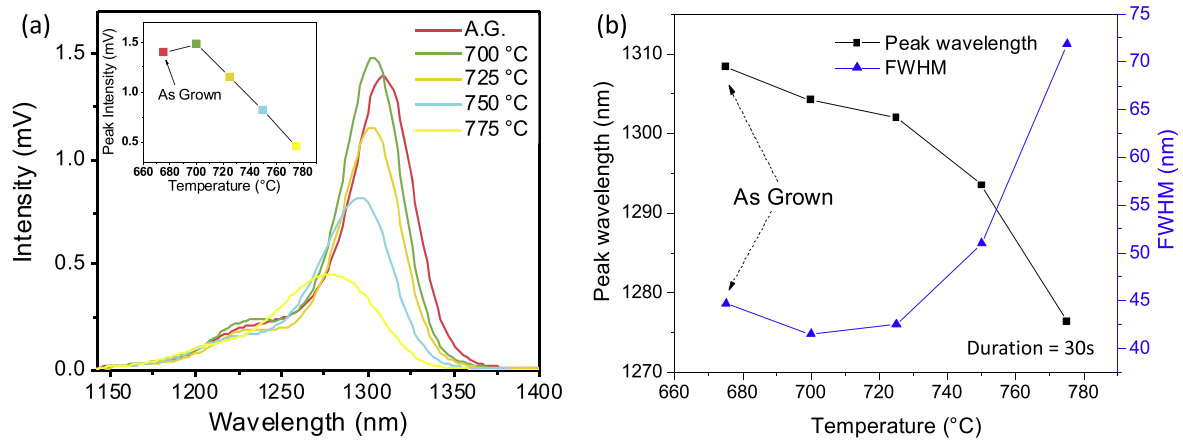


Figure 6. PL spectra of TiO₂ capped InAs/GaAs DWELL structure grown on Si substrate with 30 s duration RTA at different temperatures. Inset: the PL intensity against to the annealing temperatures. (b) Plots of PL peak wavelength and FWHM against to the annealing temperatures with 30 s duration.

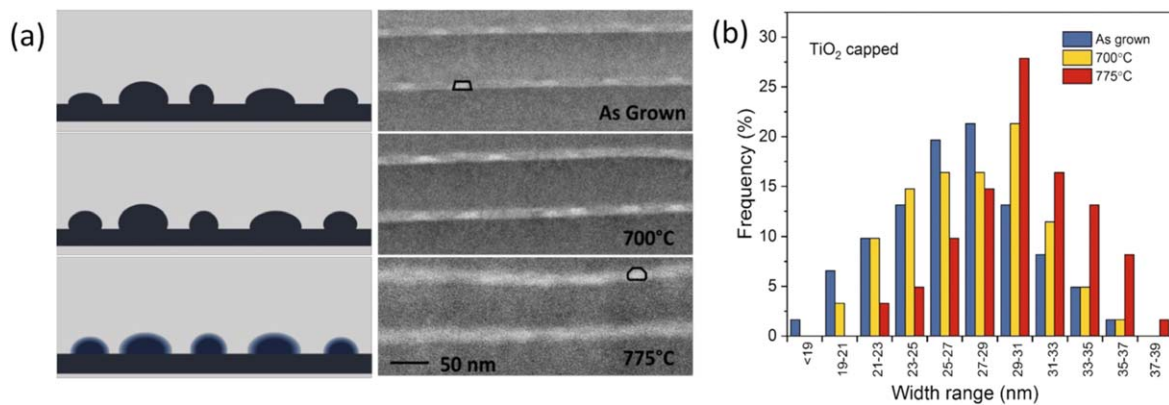


Figure 7. (a) High angle annular dark field (HAADF) STEM images of TiO₂ capped DWELL as a function of annealed temperature and related schematic diagram. (b) Histogram of TiO₂ capped QDs widths in as-grown, 700 °C annealed and 775 °C annealed samples.

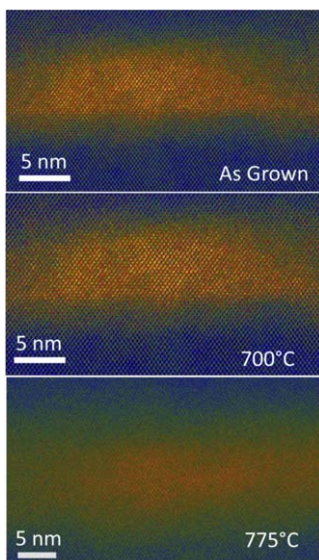


Figure 8. Cs corrected high resolution HAADF STEM images (shown in false colour) of a single QD of TiO₂ capped DWELL as a function of annealed temperature with 30 s duration.

Table 2. Summary of the widths, heights and height/width ratio of TiO₂ capped QDs in as grown, 700 °C and 800 °C annealed samples.

Sample	Width (nm)	Height (nm)	Height/width ratio
As grown	26.9 ± 3.9	8.7 ± 0.8	0.32
700 °C	27.4 ± 3.8	8.8 ± 0.8	0.32
775 °C	30.0 ± 3.4	9.0 ± 0.9	0.3

region. This RTA introduces a broader linewidth of the PL spectra for both of SiO₂ and TiO₂ capped regions. The SiO₂ region has a bigger change in FWHM and a larger blue shift compared with TiO₂. It should be noticed that, compared with the test samples in the previous studies, the real laser samples have much thicker cladding layers with high doping levels. Although we kept the other epitaxial layers and growth methods the same as the test sample, the high concentration of the dopants from the cladding layers causes an unpredicted effect on the intermixing process, with a slight material degeneration from both SiO₂ and TiO₂ capped wafer.

Figure 9(d) shows the comparison of the lasing spectra of the Si-based QD laser devices fabricated by this thermally processed wafer. Two different lasing wavelengths indicating

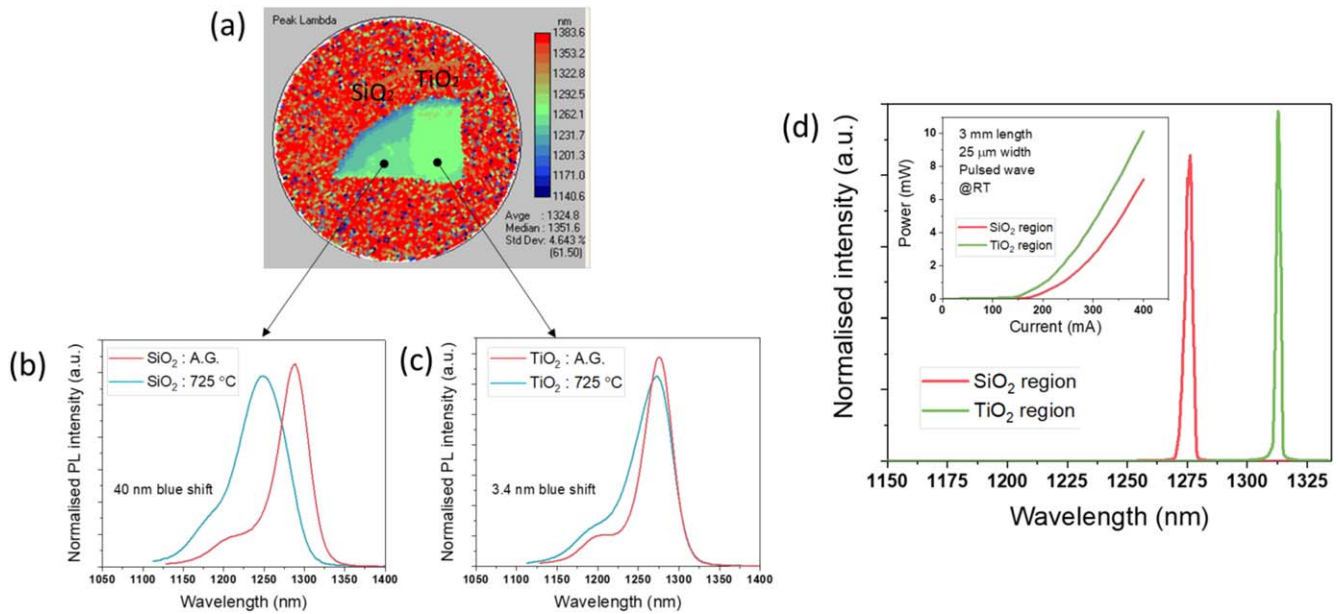


Figure 9. (a) PL mappings of InAs/GaAs DWELL laser sample on Si for selective area intermixing at 725 °C for 30 s. Comparison of PL spectra of InAs/GaAs DWELL laser sample before and after the RTA process in (b) SiO₂ capped region and (c) TiO₂ capped region. (d) Normalised emission spectra of QD lasers on Si for as grown and after the RTA process in SiO₂ and TiO₂ capped region under pulsed operation. Inset: light–current (L – I) curves of QD lasers on Si for as-grown and after the RTA process in SiO₂ and TiO₂ capped region under the pulsed-wave operation with 1% duty cycle and 1 μ s pulsed width.

Table 3. The comparison of PL parameters, in term of peak wavelength, intensity, FWHM and blue shift, for SiO₂ and TiO₂ capped DWELL structure before and after RTA with 30 s duration at 725 °C.

Sample	Peak wavelength (nm)	FWHM (nm)	Blue shift (nm)
SiO ₂ : as grown	1289.2	44.7	/
SiO ₂ : 725 °C	1249.3	72.5	40
TiO ₂ : as grown	1276.1	41.5	/
TiO ₂ : 725 °C	1272.7	57.4	3.4

the SiO₂ and TiO₂ capped regions are shown, which gives \sim 37 nm lasing wavelength difference. The inset of figure 9 is the light–current plots of the two different wavelength lasers under pulsed operation at RT with 1% duty cycle and 1 μ s pulsed width. The measured threshold currents are 150 mA and 175 mA for the TiO₂-capped and SiO₂-capped region, respectively. The single output power and slope efficiencies are 10 mW (at 400 mA) and 0.0563 W A⁻¹ for the TiO₂ region, and 7.23 mW (400 mA) and 0.0499 W A⁻¹ for the SiO₂ region. The degraded device performance from the SiO₂ capped region is related to the material degeneration from the intermixing. The TiO₂ region material has a less effect on the RTA comparing with the SiO₂ due to the suppressed inter-diffusion rate from the large thermal expansion coefficient of TiO₂.

4. Conclusion

In this paper, we have demonstrates a comparative study of intermixing effects on InAs/GaAs QDs directly grown on Si capped by separated SiO₂ and TiO₂ layers. The optimisation of annealing conditions in terms of temperature and duration

and STEM analysis were implemented for both cap materials. Electrically pumped InAs/GaAs QD lasers directly grown on Si with two different emission wavelengths of 1275 nm and 1313 nm were achieved from one single wafer by the selective area intermixing method. These results indicate that selective area intermixing is a promising technique for realising Si-based optical integrated circuits.

Acknowledgments

The authors acknowledge financial support from UK EPSRC under Grant No. EP/P006973/1, and EPSRC National Epitaxy Facility. European project H2020-ICT-PICTURE (780930), Beijing Natural Science Foundation Z180014; Royal Academy of Engineering (RF201617/16/28). ML thanks the Chinese Scholarship Council for funding her research studies. SC thanks the Royal Academy of Engineering for funding his Research Fellowship.

ORCID iDs

Mengya Liao  <https://orcid.org/0000-0002-5240-378X>Huiyun Liu  <https://orcid.org/0000-0002-7654-8553>

References

- [1] Miller D 2010 Device requirements for optical interconnects to CMOS silicon chips *Integrated Photonics Research, Silicon and Nanophotonics and Photonics in Switching* p PMB3
- [2] Rickman A 2014 The commercialization of silicon photonics *Nat. Photon.* **8** 579–82
- [3] Zhang C and Bowers J E 2018 Silicon photonic terabit/s network-on-chip for datacenter interconnection *Opt. Fiber Technol.* **44** 2–12
- [4] Liang D and Bowers J E 2010 Recent progress in lasers on silicon *Nat. Photon.* **4** 511–7
- [5] Chang H-H *et al* 2007 1310 Nm silicon evanescent laser *Opt. Express* **15** 11466
- [6] Zhou Z, Yin B and Michel J 2015 On-chip light sources for silicon photonics *Light Sci. Appl.* **4** e358–358
- [7] Tanabe K, Watanabe K and Arakawa Y 2012 III–V/Si hybrid photonic devices by direct fusion bonding. *Sci. Rep.* **2** 349
- [8] Liu H *et al* 2011 Long-wavelength InAs/GaAs quantum-dot laser diode monolithically grown on Ge substrate *Nat. Photon.* **5** 416–9
- [9] Chen S *et al* 2016 Electrically pumped continuous-wave III–V quantum dot lasers on silicon *Nat. Photon.* **10** 307–11
- [10] Chen S *et al* 2017 Electrically pumped continuous-wave 1.3 μm InAs/GaAs quantum dot lasers monolithically grown on on-axis Si (001) substrates *Opt. Express* **25** 4632–9
- [11] Wan Y *et al* 2017 O-band electrically injected quantum dot micro-ring lasers on on-axis (001) GaP/Si and V-groove Si *Opt. Express* **25** 26853
- [12] Jung D *et al* 2018 Highly reliable low-threshold InAs quantum dot lasers on on-axis (001) Si with 87% injection efficiency *ACS Photonics* **5** 1094–100
- [13] Marshall O, Hsu M, Wang Z, Kunert B, Koos C and Van Thourhout D 2018 Heterogeneous integration on silicon photonics *Proc. IEEE* **106** 2258–69
- [14] Liao M, Chen S, Park J-S, Seeds A and Liu H 2018 III–V quantum-dot lasers monolithically grown on silicon *Semicond. Sci. Technol.* **33** 123002
- [15] Liu A, Srinivasan S, Norman J, Gossard A C and Bowers J E 2015 Quantum dot lasers for silicon photonics [Invited] *Photonics Res.* **3** B1–9
- [16] Liu A Y, Komljenovic T, Davenport M L, Gossard A C and Bowers J E 2017 Reflection sensitivity of 13 μm quantum dot lasers epitaxially grown on silicon *Opt. Express* **25** 9535
- [17] Liao M *et al* 2018 Low-noise 13 μm InAs/GaAs quantum dot laser monolithically grown on silicon *Photonics Res.* **6** 1062
- [18] Inoue D *et al* 2018 Directly modulated 13 μm quantum dot lasers epitaxially grown on silicon *Opt. Express* **26** 7022
- [19] Hantschmann C *et al* 2019 Understanding the bandwidth limitations in monolithic 1.3 μm InAs/GaAs quantum dot lasers on silicon *J. Light. Technol.* **37** 949–55
- [20] Hantschmann C *et al* 2018 Gain switching of monolithic 1.3 μm InAs/GaAs quantum dot lasers on silicon *J. Light. Technol.* **36** 3837–42
- [21] Siew Ooi B *et al* 1997 Selective quantum-well intermixing in GaAs–AlGaAs structures using impurity-free vacancy diffusion *IEEE J. Quantum Electron.* **33** 1784–93
- [22] Marsh J H 1993 Quantum well intermixing *Semicond. Sci. Technol.* **8** 1136–55
- [23] Zhang G and Pessa M 1994 Thermal processing of strained-layer InGaAs/GaAs quantum well interface *Appl. Surf. Sci.* **75** 274–8
- [24] Elman B, Koteles E S, Melman P and Armiento C A 1989 GaAs/AlGaAs quantum-well intermixing using shallow ion implantation and rapid thermal annealing *J. Appl. Phys.* **66** 2104–7
- [25] Bhattacharyya D, Helmy A S, Bryce A C, Avrutin E A and Marsh J H 2000 Selective control of self-organized quantum dot properties: quantum dot intermixing *Cit. J. Appl. Phys.* **88** 4619
- [26] Ji Y, Lu W, Chen G, Chen X and Wang Q 2003 InAs/GaAs quantum dot intermixing induced by proton implantation *J. Appl. Phys.* **93** 1208–11
- [27] Zhou K *et al* 2012 Quantum dot selective area intermixing for broadband light sources *Opt. Express* **20** 26950–7
- [28] Zhang Z Y, Hogg R A, Lv X Q and Wang Z G 2010 Self-assembled quantum-dot superluminescent light-emitting diodes *Adv. Opt. Photonics* **2** 201
- [29] Zhang Z Y, Jiang Q, Hopkinson M and Hogg R A 2010 Effects of intermixing on modulation p-doped quantum dot superluminescent light emitting diodes *Opt. Express* **18** 7055
- [30] Lee H S *et al* 2009 Selective area wavelength tuning of InAs/GaAs quantum dots obtained by and layer patterning *Cit. Appl. Phys. Lett.* **94** 161906
- [31] Lee A, Jiang Q, Tang M, Zhang Y, Seeds A and Liu H 2013 InAs/GaAs quantum-dot lasers monolithically grown on Si, Ge, and Ge-on-Si substrates *IEEE J. Sel. Top. Quantum Electron.* **19** 1901107
- [32] Tang M *et al* 2016 Optimizations of defect filter layers for 1.3 μm InAs/GaAs quantum-dot lasers monolithically grown on Si substrates *IEEE J. Sel. Top. Quantum Electron.* **22** 50–6
- [33] Li W *et al* 2018 Effect of rapid thermal annealing on threading dislocation density in III–V epilayers monolithically grown on silicon *J. Appl. Phys.* **123** 215303
- [34] Xu S J *et al* 1998 Effects of rapid thermal annealing on structure and luminescence of self-assembled InAs/GaAs quantum dots *Cit. Appl. Phys. Lett.* **72** 3335
- [35] Hsu T M, Lan Y S, Chang W-H, Yeh N T and Chyi J-I 2000 Tuning the energy levels of self-assembled InAs quantum dots by rapid thermal annealing *Cit. Appl. Phys. Lett.* **76** 1987
- [36] Cusack M A, Briddon P R and Jaros M 1996 Electronic structure of InAs/GaAs self-assembled quantum dots *Phys. Rev. B* **54** R2300–3
- [37] Kim J, Wang L-W and Zunger A 1998 Comparison of the electronic structure of In As/GaAs pyramidal quantum dots with different facet orientations *Phys. Rev. B* **57** R9408–11